Article ID: 1006-8775(2011) 03-0276-09

ASYMMETRIC RAINBAND BREAKING IN TYPHOON HAITANG (2005) BEFORE AND AFTER ITS LANDFALL

DING Zhi-ying (丁治英), WANG Yong (王　勇), SHEN Xin-yong (沈新勇), XU Hai-ming (徐海明)

(Key Laboratory of Meteorological Disaster of Ministry of Education, Nanjing University of Information Science & Technology, Nanjing 210044 China)

Abstract: Using the WRF (Weather Research Forecast) model, this work performed analysis and simulation on the rainband change during the landfall of Typhoon Haitang (2005) and found that breaking may occur over land and oceans leads to distinct asymmetric precipitation. The breaking is related to the topographic effect as well as interactions between the typhoon and midlatitude systems at upper levels. During the landfall, divergent flows at the 200-hPa level of the South-Asian high combined with divergent flows at the periphery of the typhoon to form a weak, inverted trough in the northwest part of the storm, with the mid- and low-level divergence fields on the west and northwest side of the typhoon center maintaining steadily. It intensifies the upper-level cyclonic flows, in association with positive vorticity rotating counterclockwise together with air currents that travel stepwise into a vorticity zone in the vicinity of the typhoon core, thereby forming a vorticity transfer belt in 22–25° N that extends to the eastern part of the storm. It is right here that the high-level vorticity band is subsiding so that rainfall is prevented from developing, resulting in the rainbelt breaking, which is the principal cause of asymmetric precipitation occurrence. Migrating into its outer region, the banded vorticity of Haitang at high levels causes further amplification of the cyclonic circulation in the western part and transfer of positive vorticity into the typhoon such that the rainband breaking is more distinct.

Key words: typhoon; rainband; asymmetric precipitation; WRF; interactions

CLC number: P435 **Document code:** A **doi:** 10.3969/j.issn.1006-8775.2011.03.009

1 INTRODUCTION

Typhoon (or tropical cyclone, TC) rainfall is usually asymmetric, especially during its landfall. It has been actively investigated. Many studies are devoted to the impacts of different-scale interactions (Chen and Meng[1]; Tao et al.,[2]) or the relationships of interactions of the mid-level subtropical high with typhoons (e.g., Nikaidon[3]; Rodgers et al.[4]; Ren et al.[5]; Liang et al.[6]). Besides, the matching of high-and lower-level weather systems with asymmetric typhoon rainfall has been receiving more and more attention. In Zhu et al.[7], for example, based on their simulations of the evolution of the eye wall of the 1998 hurricane Bonnie and its strength, its amplification bears a relationship not only to low-level water vapor supply and warm underlying surface but also to the approaching northwesterlies at upper levels when the hurricane was deepening, and thus producing mass convergence and subsidence. It made the air warm and dry, which inhibited deep convection in the western half circle of Bonnie and resulted in asymmetricity in part of the eye wall, cloud and precipitation as well as an eastward tilt of the eye wall and storm center. The analysis demonstrated substantial influence of the variation in high-level systems on hurricane's structure and asymmetric precipitation. In their research on effects of high-level systems upon typhoon precipitation, Chinese investigators have focused on the rainfall related to TCs landing at distant locations (Sun et al.[8]; Chen and Ding[9]). In the summertime, high levels over China are under the control of the south Asian high (SAH), but generally TCs are reflected weakly in the higher troposphere. However, a typhoon, when approaching the land, has its high-level portion exposed to the effect of midlatitude systems and variations in the high-level circulations are likely to affect the distribution of TC rainbelts. But how do the high-level systems have an impact on the pattern of

Received 2010-05-21; **Revised** 2011-04-20; **Accepted** 2011-07-15

Foundation item: Natural Foundamental Research and Development Project "973" Program (2009CB421503); Natural Science Foundation of China (40975037; 40775033)

Biography: DING Zhi-ying, Professor, primarily undertaking research on mesoscale meteorology and numerical simulation.

Corresponding author: DING Zhi-ying, e-mail: dingzhiying@nuist.edu.cn

precipitation around the time when the TC makes landfall? In particular, research is little regarding the effects of interactions between the midlatitude systems and typhoon circulation at higher levels upon asymmetric rainfall happening before and after its landfall. For this reason, this study is undertaken of the variation in the Haitang rainband and the storm's interactions with the high-level midlatitude systems.

TCs are studied in the framework of WRF model-given simulations in an attempt to find out the causes of asymmetric precipitation occurring around the time when the TC landed.

2 DATA AND INTRODUTCION TO MODEL

The NCEP reanalysis data at 1° × 1° resolution were utilized with the mesoscale WRF model to simulate the Haitang rainstorm over the seaboards of Zhejiang province during 0000 UTC (Coordinated Universal Time) July 19th to 0000 UTC July 20th, 2005. The simulation schemes are presented as follows.

Dual meshes were employed, with the coarse one (181×161 gridpoints) nested with the fine one (169×196 gridpoints) at 18 (6) km spacing. With the top at 50 hPa, the model runs integration from 0000 UTC July 19th to 0000 UTC July 20th, 2005.

For the sensitivity run the terrain height was reduced below 200 m over 23–29° N and east of 110° E (figure not shown), while other conditions are the same in the control experiment. Unless stated otherwise, the analysis was made of results from the control experiment.

In situ 1-h rainfall rates taken at 3-h intervals came from the automatic weather stations (AWS), with reference to TRMM gridded precipitation at 25×25 km spacing.

3 SIMULATED RAINFALL AND TYPHOON TRACK COMPARED WITH OBSERVATIONS

Comparisons between simulated 24-h fine-mesh precipitation starting from 0000 UTC July 19th (Fig. 1a) and the measured (Fig. 1b) yields two simulated centers of >300 mm (121° E, 28.2° N, and 120° E, 27.2° N) that are close to the in situ observed counterparts (120.5° E, 27.5° N, and 121° E, 28.2° N). For the simulation, the former rainfall center appeared mainly over 0000–0900 UTC July 19th and latter over 0500–1600 UTC July 19th; for the observation, the former rainfall center maintained over 0000–0600 July 19th and latter over 0600–1800 UTC, July 19th. The duration was close to to the observations, but the latter modeled precipitation was slightly smaller compared to the measurement while the former was much closer.

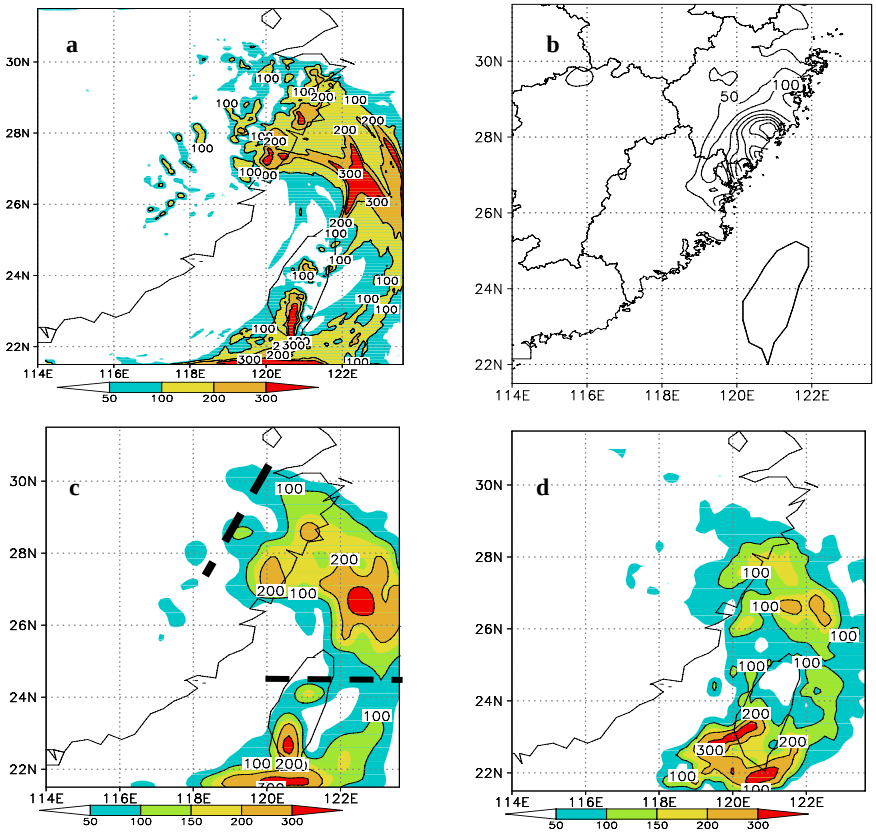

Fig.1. 24-h rainfall during 0000 UTC July 19th to 0000 UTC July 20th, 2005 (unit: mm). a: fine-mesh simulations; b: observations (at 50 mm intervals); c: coarse-mesh simulations (broken line refers to rainband breaking); d: TRMM sensings

As no rainfall records were available over the sea for validation, the 1-h gridded data at 0.25° ×0.25° lat./long., provided by TRMM, were employed (Fig. 1d) for comparison. The figure shows that the strong rainfall zones over the coastal bands were, in most cases, detected, with the intensity somewhat lower than the AWS records. Where the measured precipitation exceeded 300 mm, the radar-given maximum measurement was lower than 250 mm, suggesting that the radar-located position was basically correct but its measurement was lower compared to the AWS records. Since the rainfall-measuring radar gave a relatively correct location of the intense rainfall center, its measurements could be utilized as reference for rainfall of marine zones and its relative value. Examination of Figs. 1a and 1d reveals that the precipitation was simulated over the sea south of 26° N around 122° E, with the intensity higher than radar estimates. Besides, the simulated position and strength of the precipitation south of Taiwan were relatively realistic. As a result, the simulations are reasonable. The 24-h coarse mesh (18 km × 18 km) simulated rainfall is quite similar to that from TRMM probings (25 km×25 km) in Fig.1c.

Figure 1 depicts two distinct features of rainfall fields, confirmed by either observations, TRMM sensings or simulations from the coarse or fine mesh model. One is the noticeable discontinuity arising in the rainbelt to the west of the strongest precipitating center over the land, and the other is the existence of two cores of heavy rain clusters to the north and south of Taiwan, with rainfall reduced greatly in between (indicated by the broken line in Fig. 1c). The 1-h simulated precipitation pattern shows that the rainband is continuous prior to 0800 UTC July 19th (see Figs. 2a & 2b) and a break happens at model hour 0800, followed by an increasingly bigger split, as clearly revealed on the TRMM image (figure not shown). Why did the rainbelt break in that place and what was the cause of the break? We shall deal with the problems in following sections.

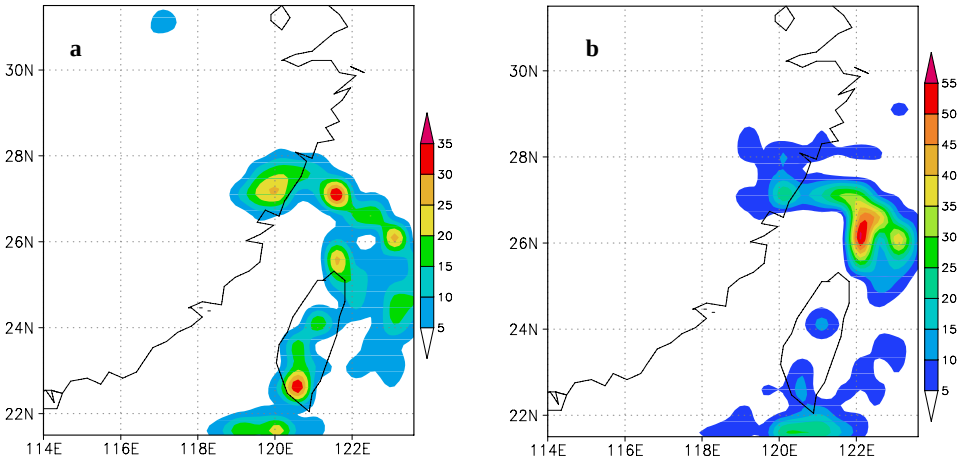

Fig. 2. 1-h rainfall based on 4-h integration (a) and 8-h integration (b) over the coarse mesh.

This simulated geometry is broadly consistent with the observed (Wang and Ding[10]). The simulation is successful in terms of the simulated track and precipitation so that it can be employed for further analysis. Coarse-mesh rainfall is close to the TRMM data but there are no in situ observations over the sea to validate the simulations. The following discussion will be based just on coarse-mesh imitations, unless otherwise mentioned.

4 ANALYSIS OF THE CAUSES OF RAINBAND BREAKING

The 24-h vorticity variation around 25° N,123° E (Fig. 3a) starting from 0000 UTC July 19th shows the strongest vorticity at lower levels to be at model hours 0000–0800, indicating a positive vorticity core around 700 hPa and weaker negative vorticity above it. The integration at model hour 0900 presents a more intense positive vorticity center at 150 hPa, with a central value of $20\times10^{-5}s^{-1}$, maximizing at $30\times10^{-5}s^{-1}$ at model hour 1300. In contrast, the low-level vigorous vorticity weakened greatly in that period. From model hours 1400 to 1700 negative vorticity emerged at 200 hPa while low-level vorticity amplified to some extent. As time went on, the 200-hPa level was largely under the control of positive vorticity. As seen from the evolution of vertical velocity in Fig. 3b, although descending motion appeared in the 200-hPa strong vorticity zone, ascending motion remained below 300 hPa and reduced greatly, compared to the situation prior to model hour 0600. Appearance of vigorous vorticity at 200 hPa led to subsidence, preventing the rising motion from intensification inside the typhoon. It was due to the weakened rising that resulted in the

breaking of the rainbelt. As to the formation of 200-hPa vorticity, it will be discussed later.

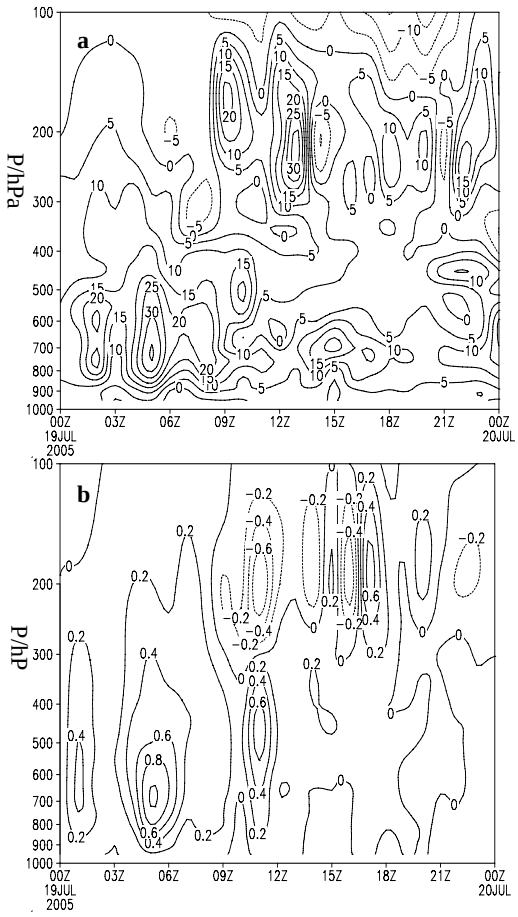

Fig. 3. The time–pressure cross section of vorticity ($10^{-5}s^{-1}$) around 25° N, 123° E in (a), and vertical speed (m/s) in (b) for 0000 UTC July 19th through 0000 UTC July 20th.

Examination of 24-h fine-mesh rainfall (Fig. 1a) indicates that precipitation occurred dominantly over the seaboard during landing. To the west there were banded hyetal zones alone, which were more evident in the fine-mesh simulations (figure not shown), as demonstrated on the TRMM image. Note that the rainband breaking on land differed from that over the sea, likely because the hilly seaboard might act as the barrier that gave rise to the breaking. The wind difference (200 hPa minus 850 hPa) shows the shearing of the environmental winds that directed towards the southwest (indicated by the arrow points in Fig. 8c), where we see most rainbelts to the left of the shear line in the downwind direction, in good agreement with findings in previous studies (DeMaria[11]; Frank and Ritchie[12]; Corbosiero and Molinari[13]). The breaking over the coastal belt may be associated with the unique distribution of the environmental winds, though it fails to interpret the distinct breaking over waters and the existence of precipitating areas to the west of the typhoon's center over land. Around the time of landfall, the TC, when approaching the land, was affected by continental systems. Especially its high-level features (e.g., vigor and extent) were much weaker as compared to those at lower levels, suggesting that midlatitude systems in the higher troposphere have stronger effect on the typhoon. How did the high-level systems influence the distribution of rainbands and what were the interactions between the typhoon and the systems? These key issues will be examined subsequently.

4.1 *The rainbelt breaking associated with systems at high and lower levels*

The 850-hPa convergent flow field matches the 200-hPa divergent field, to the east of the TC center (see Figs. 4a & 4b), and the low-level divergent flow field matches the 200-hPa convergence, to the west of it. The 200-hPa flow field was only a northward-extending inverted trough at 0000 UTC July 19th, which was formed by a combination of divergent air out of the typhoon with flows at the periphery of SAH (Fig. 5a). As shown by the mean divergence field over 22–30° N, 111–116° E on the west side of the typhoon, the lower-level divergence is much stronger than the upper-level convergence at model hour 0600. At model hour 0800, the strongest convergence center emerged at 500 hPa and after model hour 0900 the 200-hPa convergence was greatly reinforced, with divergence prevailing at mid- and lower-levels. The initial divergence dominated lower levels to the west of the TC center and the 200-hPa convergence began to strengthen after model hour 0600. Subsequently, at model hour 0900, the strongest convergence center emerged at 150 hPa and maintained there. Inspection of the evolution of the 850-hPa circulation (Figs. 4a & 4c) yields that from 0000 UTC July 19th to 0000 UTC July 20th its change was smaller in sharp contrast to the 200-hPa counterpart. The inverted trough, previously in the outer-region of the typhoon, developed into a big cyclone with three cores (Figs. 4b & 4d). Core A coincides with the original TC center and Cores B and C are cyclonic centers to the west of the eye. Following the compensation principle, the low-level steady divergence favors the formation of a high-level convergence field and cyclonic circulation center. Analysis of the vertical speeds on the west side of the typhoon's core indicates that subsidence is predominant to the west of the TC center (Fig. 5b), which is the principal cause of unlikely precipitation over the area.

Then, is the development of the 200-hPa cyclonic circulation center related to the breaking of the spiral rainband over the sea? As shown earlier (Wang and Ding[10]), the cyclonic circulation formation, owing to the gradual amplification of the typhoon after its landfall, is most likely attributable to the existence of divergence fields at mid- to lower-levels to the west of

the typhoon. As depicted in Fig. 4d, the distinct breaking of the rain zone is seen to the north of Taiwan. There is noticeable cyclonic shearing at 200 hPa, where the cyclonic shearing convergence leads to convergent-flow subsidence to prevent rainfall from formation (Fig. 5b). Consequently, another cause of the breaking is likely to be associated with the cyclonic shearing generated at 200 hPa.

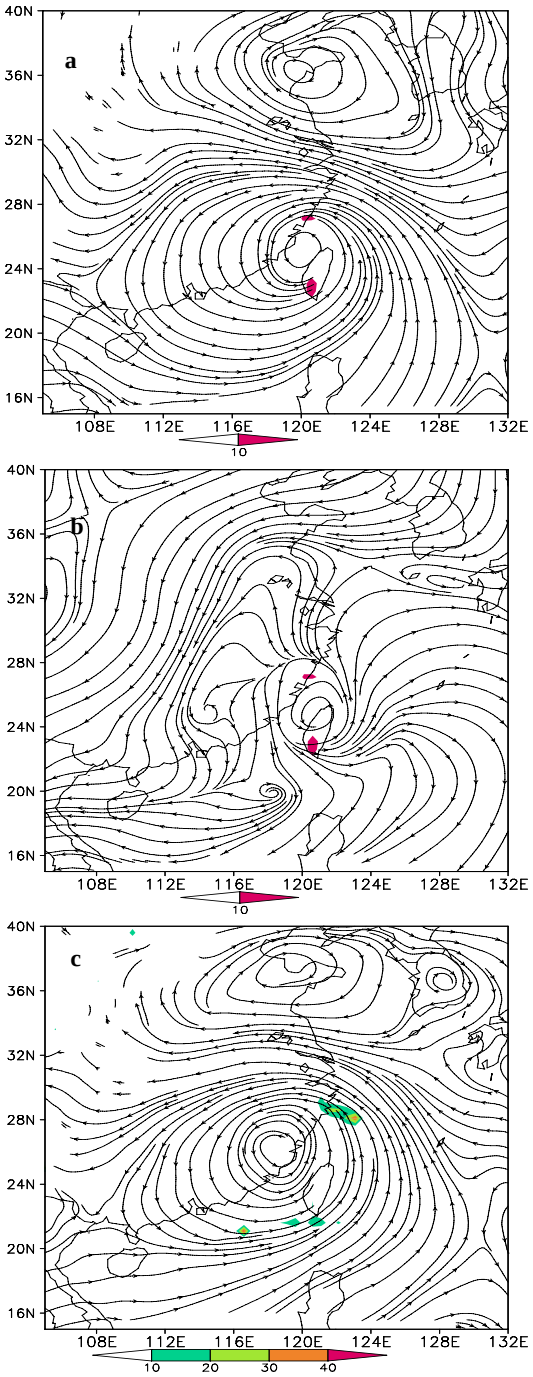

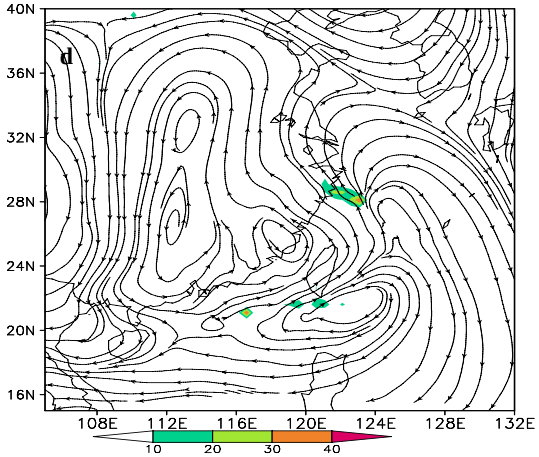

Fig. 4. The initial flow field at 850 hPa (a) and 200 hPa (b) at 0000 UTC July 19th and the forecast flow field for 200 hPa (a) and 850 hPa (d) at 0000 UTC July 19th, 2005, with 1-h rainfall areas shaded.

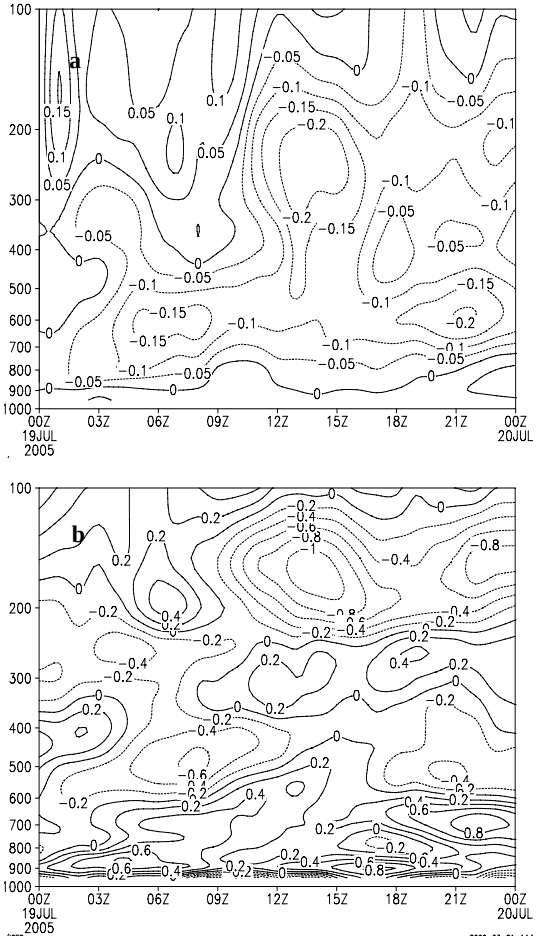

Fig. 5. The time-pressure cross section of the divergence field in (a) and vertical speeds in (b) averaged over 22–30° N, 111–116° E for 0000 UTC July 19th to 0000 UTC July 20th, with the same units as given in Fig. 4.

From the circulation and vorticity (1-h integrations) distributed initially at 200 hPa (Fig. 6a), we see that in the initial field there is a positive vorticity core to the north of the eye in 35° N, 117° E

and the positive vorticity zone extends as far as around 22° N (called region B), with a vigorous positive vorticity center residing over the TC core. The TC core is unrelated to the vorticity zone outside the typhoon, indicating that the TC vorticity field has no relation to midlatitude systems in the initial field, with the rain-forming zone at the brim rather than in the vorticity zone. Afterwards, region-B vorticity develops steadily, with a branch of vorticity migrating southeastward and the TC vorticity spreading outward. At model hour 0400 (Fig. 6b), to the northwest, the TC vorticity zone connects with the region-B counterpart (indicated by arrow in Fig. 6b). The region-B vorticity grows to a certain extent (with the approaching of a positive vorticity band from model hour 0400–1500 as in Fig. 7a), and connects with the positive vorticity band by stretching toward the south, forming a strong positive vorticity passage in 22–25° N, allowing midlatitude vorticity to come into the TC core on a continuous basis. It is discerned at higher-than-400-hPa levels, as given in Fig.7b, with a positive vorticity zone in 200–400 hPa, above which the strongest core travels east as a function of time (figure not shown). There are vigorous positive vorticity and wind shear in the direction in the pronounced breaking of the rainband to the east of the TC center, which are, obviously, owing mainly to the steady transfer of midlatitude vorticity. Intense precipitation occurred in the divergent flows at the fringe of the vorticity passage. At model hour 1800 (Fig. 4d), the TC circulation merges with the midlatitude circulation to form a large-scale cyclonic circulation in the higher troposphere.

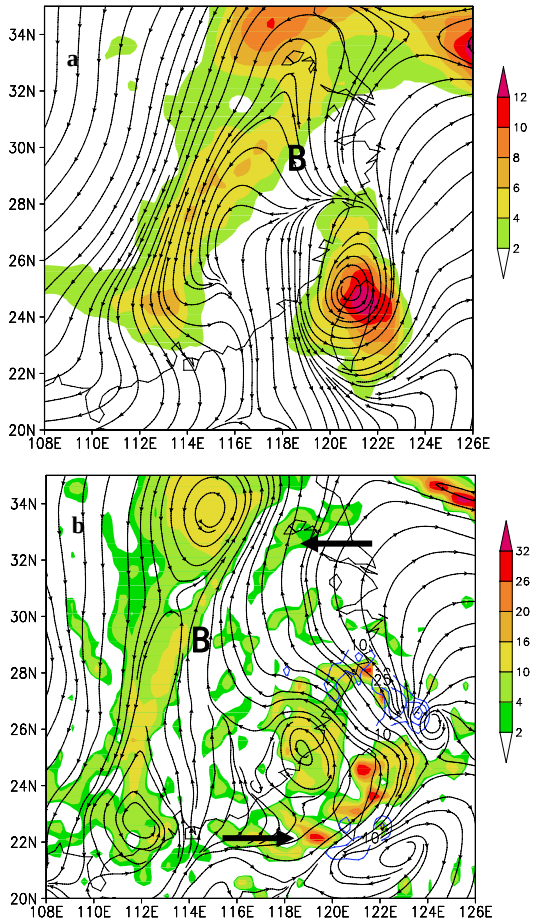

Fig. 6. Distribution of positive vorticity ($10^{-5}s^{-1}$) for the circulation field at 1-h (a) and 12-h (b) integration at the 200-hPa coarse mesh. Solid line: 1-h isopluvial; arrow: moving direction of the positive vorticity

In order to clearly show the relationship between the vorticity field of typhoon and that of the midlatitude system, the five terms to the right of the equation are shown as follows:

$$\frac{\partial \varsigma}{\partial t} = -(u\frac{\partial \varsigma}{\partial x} + v\frac{\partial \varsigma}{\partial y}) - (u\frac{\partial f}{\partial x} + v\frac{\partial f}{\partial y}) - \omega\frac{\partial \varsigma}{\partial p} + (\frac{\partial \omega}{\partial y}\frac{\partial u}{\partial p} - \frac{\partial \omega}{\partial x}\frac{\partial v}{\partial p}) - (f+\varsigma)(\frac{\partial u}{\partial x} + \frac{\partial v}{\partial y})$$

(1) (2) (3) (4) (5)

The calculation and analysis of magnitude order shows that term (1) and term (5) in the equation matter most to the vorticity, which will be discussed in the following section. In Fig. 7c, prior to the model hour 1500, positive vorticity advection is the main form in 33° N and positive vorticity advection strengthens the vorticity there (Fig. 7a). 15 hours later, the negative vorticity advection becomes dominant and the increase of positive vorticity is mainly shown in the divergence and absolute vorticity terms. The convergence in the upper level strengthens the positive vorticity. The vorticity advection is mainly positive at 22° N (Fig. 7d), but still with obvious fluctuation. The intense positive-vorticity advection is in coincidence with high vorticity value and sinking air flow, while intense negative vorticity advection (at model hour 1400) is with high negative vorticity and upward movement (Figs. 3a & 3b). The divergence and absolute vorticity terms exert negative influence on the vorticity.

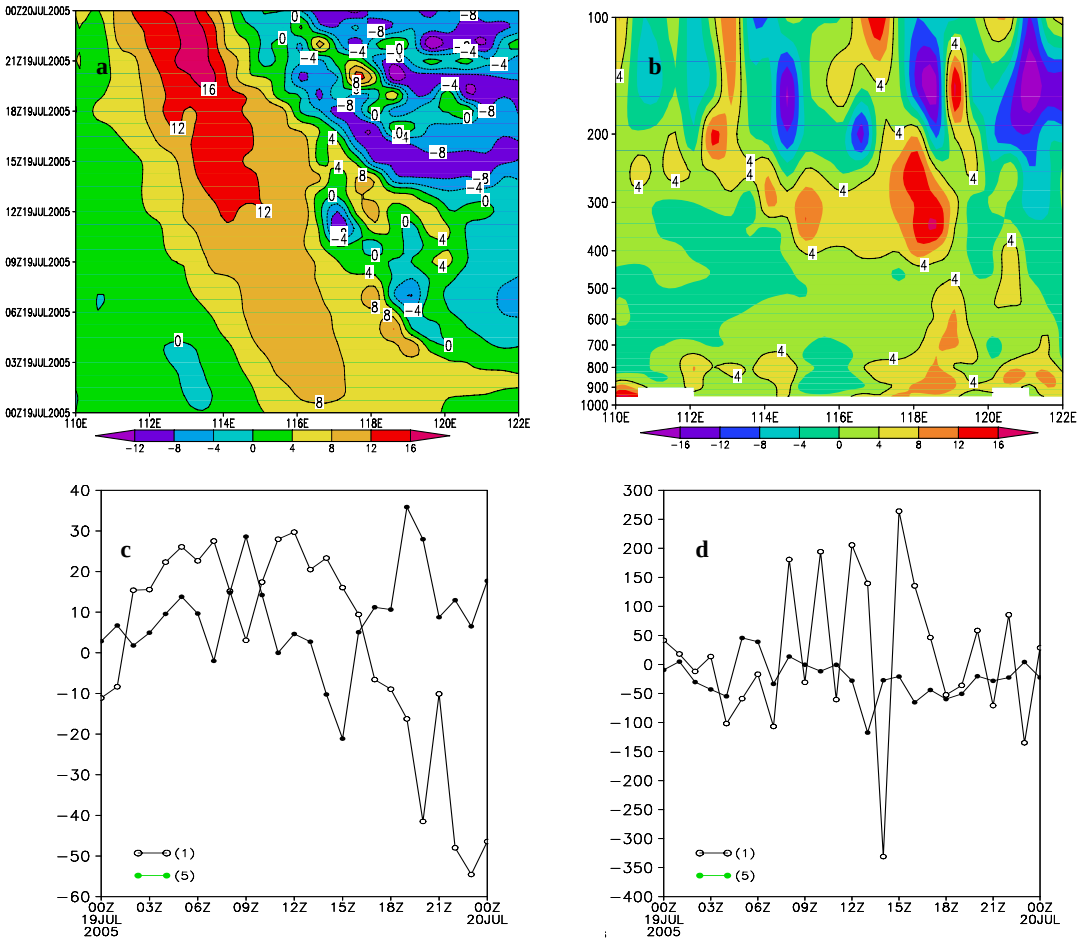

Fig. 7. Evolution of 200-hPa vorticity along 33° N during 0000 UTC July 19th to 0000 UTC July 20th (a); 22° N cross section of vorticity from a 15-h integration (b); evolution of terms (1) and (5) of the equation with time from 0000 UTC July 19th to 0000 UTC July 20th at 200 hPa along 33° N, 113–115° E (c) and 25° N, 121–123° E (d). unit: $10^{-10}s^{-2}$

Based on the foregoing analysis, we see that around the time of landfall of the TC, due to the closeness to and interactions with midlatitude systems, 200-hPa TC circulation has more significant interations with midlatitude systems. The positive vorticity field diverges outward, resulting in the development of an inverted trough in the midlatitudes, which in turn forms a passage there to allow positive vorticity to be transferred into the TC region, thereby making the rainband break. No precipitation is formed below the 200-hPa vorticity zone. The maintenance of the low-level divergence field of the TC also contributes to the cyclonic circulation in the higher troposphere (Fig. 5).

4.2 *Relation of topographic features to the breaking of spiral rainband*

To investigate the relationship of the topography with the breaking, we conducted a sensitivity experiment with the terrain height reduced below 200 m. Under the assumption of the surface features in eastern China and northern Taiwan (as shown in Fig. 8a), we compared the 24-h rainfall with the output of the control run (Fig. 1c). The breaking on land remained evident, but the multiple disturbance rainfall centers—originally on the east side of land intense precipitation bands—were no longer available, as clearly seen on the 1-h rainfall map (Figs. 8c & 8d). The marine breaking was still existent and the 28° N hyetal zone moved westward over some distance, but the breaking bands migrated slightly southward, as shown from the comparison of total precipitation. The breaking still occurred over land and sea despite the lowered surface features except that the disturbance rainband practically disappeared over land (Fig. 9). It follows that surface features have a great impact on the disturbance rainbands. With lowered surface features, the rainfall reduced greatly in intensity over the seaboard, indicating that the original topography played a significant role in augmenting precipitation due to its lifting of air (Zhang et al.[14]; Ji et al.[15]; Liang et al.[16]). Analysis also suggests that the topography made minor contribution to the breaking.

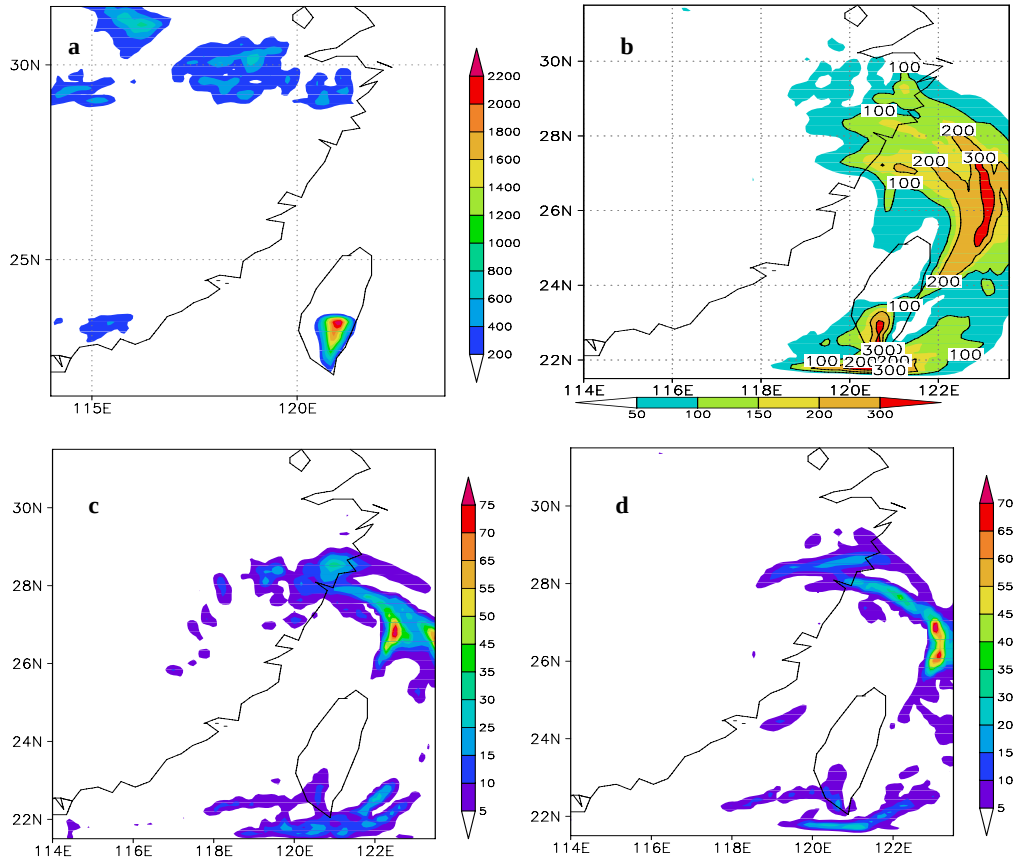

Fig. 8. (a) Simulation with surface features removed; (b) rainfall during 0000 UTC July 19th–0000 UTC July 20th from the terrain-sensitive experiment ; (c) distribution of precipitation at the 12th hour in the control run; (d) rainfall at the12th hour from the terrain-sensitive experiment. Units: mm

The analysis shows that during the experiment, in the divergence field at 850 hPa (Fig. 9), the convergence band appears over the sea, with a scattered westen convergence field in the TC center (Fig. 9a). With lowered surface features, the convergent flow field weakens greatly (Fig. 9b), which shows that the lowering of the surface features would not strengthen the convergent flow field. Topography can strengthen the westen convergence field in the TC center, forming banded rain fields, which could be related with gravity waves.

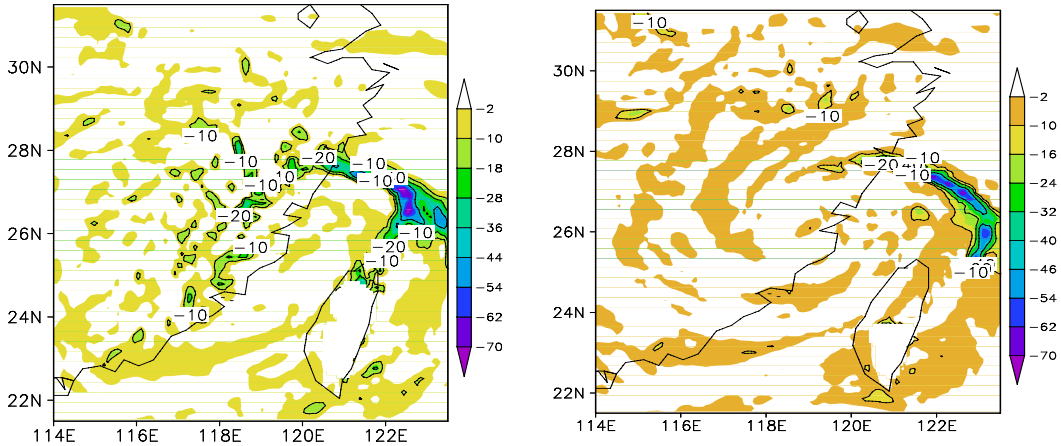

Fig. 9. Convergent band of 850-hPa divergence at the 10th hour from the control run (left panel) and from the sensitivity experiment with terrain removed (right panel). Units: $10^{-5}s^{-1}$

5 CONCLUDING REMARKS

Based on the foregoing analysis, the following points can be concluded.

(1) The reduced-terrain-height sensitivity experiment shows that the topography exerts minor influence on the breaking of a rainbelt. With such surface features adopted, the rainband extends marginally westward in a less discrete way, indicating that surface features play a greater part in forming land disturbance rainbands. The complicated topography could strengthen the convergence band in the low level, therefore bringing about disturbance rainbands while exerting mild influence on the breaking of the rainband at sea.

(2) The 200-hPa positive vorticity field prevents rainfall from development, with precipitation happening dominantly outside the vorticity zone. Interactions between cyclonic flow fields of the typhoon at 200 hPa and those of midlatitudes have considerable impacts on the breaking of the spiral rainband. Around the time of landfall, the mid- and lower-level divergence fields to the west and northwest of the TC center cause the generation of positive vorticity and cyclonic stream fields at 200 hPa; the vorticity zone rotates counterclockwise with airflows, merging with the TC's vorticity field to form a positive vorticity passage directed toward the TC. It increases the 200-hPa cyclonic vorticity and wind shear to the east of the TC center, accompanied by subsidence that gives rise to the breaking, a main cause of the asymmetric precipitation. The TC positive vorticity, when spreading outward as waves, meets and merges with the vorticity zone to the west, causing the cyclonic circulation there to be further amplified and the circulation, when combined with the TC circulation, forms a vigorous 200-hPa cyclonic circulation that is liable for transferring more positive vorticity into the TC, leading to more significant breaking of the rainbelt.

(3) During the landfall, the TC intensity and its influencing extent are much smaller at 200 than at 850 hPa so that the 200-hPa TC portion is subject to the effects of midlatitude circulations, especially in eastern Asia, where the SAH is rather strong at the upper level and influences a larger portion of the TC; both of them are interacting to affect the typhoon rainfall more pronouncedly. In this case, the stable divergent air flow in the low level of the TC, together with outside divergence of its positive vorticity field, brings about the inverted trough in the midlatitudes, which in turn forms a passage at midlatitudes to allow vorticity to be transferred into the TC region, thereby making the rainband break.

REFERENCES:

[1] CHEN Lian-shou, MENG Zhi-yong. Advances in tropical cyclones in China over the past decade [J]. Chin. J. Atmos. Sci., 2001: 25 (3): 420-432 (in Chinese).
[2] TAO Zu-yu, TIAN Bai-jun, HUANG Wei. The asymmetric structure and rainstorm for the landing typhoon coded as 9216 [J]. J. Trop. Meteor., 1994: 10: 69-77 (in Chinese).
[3] NIKAIDON Y. The PJ-like north–south oscillation spectral model T42 [J]. J. Meteor. Soc. Japan, 1989: 67, 687-704.
[4] RODGERS E B, JONG J B, HAROLD F P. The environmental influence on tropical cyclone precipitation [J]. J. Appl. Meteor., 1996: 33 (5): 573-593.
[5] REN Su-ling, LIU Yi-min, WU Guo-xiong. Numerical study of interactions between the western Pacific subtropical high and typhoon [J]. Acta Meteor. Sinica, 2007: 65(3): 329-340 (in Chinese).
[6] LIANG Li, WU Zhi-wei, YAN Guang-hua. The dynamic mechanism of the maintenance after the landing of the tropical cyclone 9012 [J]. J. Trop. Meteor., 1995, 11(1): 26-34 (in Chinese).
[7] ZHU T, ZHANG D L, WENG F. Numerical simulation of hurricane Bonnie in 1998. Part I: Eyewall evolution and intensity changes [J]. Mon. Wea. Rev., 2003: 132, 225-241.
[8] SUN Jian-hua, QI Lin-lin, ZHAO Si-xiong. Study of exceptionally strong rainstorm causing meso convective system in north China associated with typhoon coded as 9608 landing and migrating northward [J]. Acta Meteor. Sinica, 2006: 64 (1): 57-71 (in Chinese).
[9] CHEN Jiu-kang, DING Zhi-ying. On a meso rainstorm system from the coupling of high- and low-level jets with the typhoon circulation [J]. Quart. J. Appl. Meteor., 2000, 11(3): 272-281 (in Chinese).
[10] WANG Yong, DING Zhi-ying. Dynamic analysis of asymmetric spiral rainbands around the landing of typhoon Haitang [J]. J. Nanjing Inst. Meteor., 2008: 31(3): 352-362.
[11] DeMARIA M. The effect of vertical shear on tropical cyclone intensity change [J]. J. Atmos. Sci., 1996, 53: 2067-2087.
[12] FRANK W M, RITCHIE E A. Effects of environmental flow upon tropical cyclone structure [J]. Mon. Wea. Rev., 1999, 127: 2044-2061.
[13] CORBOSIERO K L, MOLINARI J. The effects of vertical wind stress on distribution of convection in tropical cyclones [J]. Mon. Wea. Rev., 2002: 130, 2112-2113.
[14] ZHANG Jian-hai, CHEN Hong-mei, CHU Xiao-ming. Numerical simulation of topographic impacts on the typhoon Haitang (coded 0505) during its landfall [J]. Bull. Oceanogr., 2006, 25(2): 1-7 (in Chinese).
[15] JI Chun-xiao, XUE Gen-yuan, ZHAI Fang, et al. Numerical experiment in effects of terrain upon the rainfall structure for typhoon Rananim in its landing [J]. Chin. J. Atmos. Sci., 2007, 31(2): 233-244 (in Chinese).
[16] LIANG Jian-yin, CHEN Zi-tong, WAN Qi-lin, et al. The diagnostic analysis of the landing of tropical cyclone Vongfong [J]. J. Trop. Meteor., 2003, 19(suppl.): 45-55.

Citation: DING Zhi-ying, WANG Yong, SHEN Xin-yong et al. Asymmetric rainband breaking in Typhoon Haitang (2005) before and after its landfall. *J. Trop. Meteor.*, 2011, 17(3): 276-284.